ACS OMEGA

Article

Cite This: ACS Omega 2019, 4, 11082−11092

http://pubs.acs.org/journal/acsodf

Experimental Study on the Density-Driven Carbon Dioxide Convective Diffusion in Formation Water at Reservoir Conditions

Yongqiang Tang,[†] Zihao Li,[‡] Rui Wang,[†] Maolei Cui,[†] Xin Wang,[†] Zengmin Lun,[†] and Yu Lu*[,§]

[†]Petroleum Exploration and Production Research Institute, Sinopec, Beijing 100083, China

[‡]Department of Mining and Minerals Engineering, Virginia Tech, Blacksburg, Virginia 24061, United States

[§]School of Business, Beijing Technology and Business University, Beijing 100048, China

ABSTRACT: Density-driven convection, which can accelerate the dissolution rate of carbon dioxide (CO_2) in resident brine, is critical for the long-term fate of the injected CO_2 permanence and security of CO_2 geological storage. Visualization experiments and pressure−volume−temperature (PVT) testing were conducted to investigate the influence from gravitational convection. For investigate gravitational instabilities and convective diffusion, we designed a Hele-Shaw cell rated to 70 MPa and Rayleigh number of 346 to conduct visualization experiments with the micro-schlieren technique. The average diffusion coefficient and time-dependent values were measured in the PVT experiments. We also calculated the convection parameters, including Rayleigh number and critical onset time, with a series of PVT testing at the temperature ranging 293.15−423.15 K and pressure ranging 14−24 MPa by using the constant-pressure method. Through visualization experiments, we observed convective currents triggered by the density gradient in the gas−liquid interface, which noticeably enhanced the CO_2 dissolution rate. The PVT testing confirmed that the diffusion coefficient increased sharply under the influence of the gravitational convection at the early stage and then decreased toward the average diffusion coefficient with time. The PVT testing also demonstrated the Rayleigh number increasing with temperature or pressure increasing under the reservoir conditions. The gravitational convection will be more likely to occur and more rapid with a greater pressure or higher temperature.

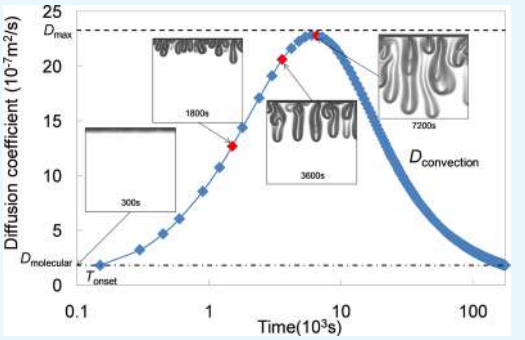

INTRODUCTION

Gravitational Convection. The growing concern about CO_2 emission urged people to investigate the solutions of CO_2 over emission. CO_2 geological storage in the aquifers or depleted oil reservoirs is one of the optimal techniques to prevent CO_2 from entering the atmosphere.[1,2]

Dissolution trapping is an important mechanism, which usually captures two-thirds of the total storage volume.[3,4] The molecular diffusion of CO_2 in brine is woefully slow.[5] The key issue for accurate assessment of the dissolution trapping is the dissolution rate. As illustrated in Figure 1, many mechanisms accelerate the diffusion of CO_2 in brine and involve dispersion,[6] advection, and gravitational convection.[7]

Among these mechanisms, advection is the dominant driving force because lower vertical permeability may reduce the gravitational convection while potentially increasing transverse mixing.[9] Nevertheless, the gravitational convective diffusion can greatly enhance the CO_2 mixing efficiency, storage capacity, and mass transfer rate.[10] Gravitational convection mitigates the risk of CO_2 leakage to provide a long-term storage security[11] by driving CO_2 sinking rather than rising to shallower formations. Therefore, gravitational convection is critical for the long-term fate of CO_2 and the security of storage.[1,8]

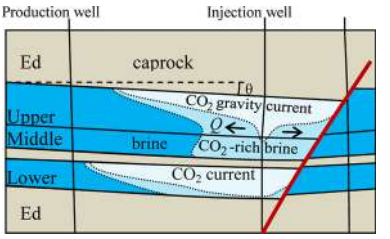

Figure 1. Schematic illustration of fluid dynamics and trapping associated with CO_2 geological storage in real formation, wherein the free CO_2 can be laterally displaced beneath the caprock[8] by combinations of the volumetric flux of injected CO_2 (Q) and the aquifer slope (θ).

Convective Parameters. The CO_2 dissolution can result in a 2−3% density increase of brines;[12] the slight increment of density in brine will lead to gravitational instability[9,13] and convection currents.[10,14] Moreover, the convection will accelerate the dissolution of CO_2 into the brine, further enhance the mass transfer rate, and shorten the dissolution time.[15] The density-driven convection is sometimes referred to

Received: March 6, 2019
Accepted: June 11, 2019
Published: June 25, 2019

DOI: 10.1021/acsomega.9b00627
ACS Omega 2019, 4, 11082−11092

as Rayleigh–Taylor instability.[9] Based on the Boussinesq approximation, the density-driven flow can be described as a mixed equation of the mass conservation equation and Fick's second law[16]

$$\frac{\partial c(x,t)}{\partial t} + v\frac{\partial c(x,t)}{\partial x} - D\frac{\partial^2 c(x,t)}{\partial x^2} = 0 \quad (1)$$

where v is the velocity (or volume-averaged velocity).

The incompressible Navier–Stokes equation can describe the density-driven convective diffusion as

$$\frac{\partial v}{\partial t} = -\frac{1}{\rho}\nabla P + \frac{\mu}{\rho}\nabla^2 v + g \quad (2)$$

The most common criterion to indicate the occurrence of natural convection is Rayleigh number (Ra_c),[17] which is a dimensionless measure as a ratio of free convection to diffusion[7,8]

$$\mathrm{Ra} = \frac{K\Delta\rho g H}{\varphi\mu D} \quad (3)$$

where K is the effective permeability; $\Delta\rho$ is the excess density of CO_2-rich brine over fresh brine; g is the gravitational acceleration (g = 9.8015 m/s^2 in Beijing); H is the vertical thickness of diffusion, which is less the height of model; ϕ is the porosity; μ is the viscosity of CO_2-rich brine; and D is the CO_2 diffusion coefficient.

For a Hele-Shaw cell with uniform aperture thickness, the porosity is 1, and its effective permeability can be calculated as[18,19]

$$K = b^2/12 \quad (4)$$

where b is the aperture thickness of the Hele-Shaw cell.

Only when the diffusive layer becomes thick enough that the Rayleigh number exceeds a critical value (Ra_c); the gravitational instabilities can be triggered by perturbations in the diffusion layer.[20] Nield[21] offered a method to measure the critical value under various boundary conditions. The critical Rayleigh number is 32.5 as estimated by Slim and Ramakrishnan[22] based on the linear stability analysis, 55 as estimated by Szulczewski et al.,[23] and 31.5 as estimated by Slim[24] through the theoretical analysis of the dissolution rate. Some studies[7,16,25] suggested that the appropriate critical value should be $4\pi^2$ with the associated critical wavenumber (λ_c) of π, which is also used in this paper.

A critical onset time (t_c) and critical wavelength (λ_c) were widely used to predict the gravitational instabilities. Both the onset time and critical wavelength depend on porosity and permeability.[14]

The critical onset time t_c can be predicted as[20]

$$t_c = \alpha_1 D\left(\frac{\varphi\mu}{K\Delta\rho g}\right)^2 \approx \alpha_2 \mathrm{Ra}^{-2} \quad (5)$$

where α_1 and α_2 are the parameters for the onset time of convection. The parameter α_1 is 130 as reported by Hassanzadeh et al.[26] The parameter α_1 offered by Teng et al.[27,28] is 48.7. We believe that the parameter α_1 should range from 45 to 130.

The critical wavelength λ_c can be calculated as

$$\lambda_c = \frac{a_3 D\varphi\mu}{K\Delta\rho g} \quad (6)$$

It is reported that the density-driven convection enhances the CO_2 dissolution rate with the increase in Rayleigh number.[29] Islam et al.[5] indicated that effective convection occurred only at a limited range of scales when Rayleigh numbers exceeded the critical value.

Hele-Shaw Experiments. Visualization study with the Hele-Shaw cell[30] apparatus is one of the primary methods used to investigate the mechanisms of the CO_2 natural convection. Kneafsey and Pruess[25] once performed CO_2 convective dissolution in transparent vertical Hele-Shaw cells that contained water overlain by a gas phase at atmospheric pressure. Backhaus et al.[31] investigated the instability of initial convective dissolution with a Hele-Shaw cell (6000 < Ra < 90000) to determine the rates of CO_2 dissolution trapping in brine at atmospheric pressure. Slim et al.[18] described the CO_2 convection behavior in brine from the first contact to 65% average saturation with a Hele-Shaw cell (100 < Ra < 1700) at atmospheric pressure. Mojtaba et al.[32] observed the convective instabilities of CO_2 in a Hele-Shaw cell (182 < Ra < 20860) under 3.45 MPa. Vosper et al.[33] studied the process of CO_2 dissolution and convection in water under low pressure with a Hele-Shaw cell filled with transparent glass beads. Faisal et al.[19] used a catalytic combustion-based total carbon analyzer to determine CO_2 mass transfer in a Hele-Shaw cell (3277.88 < Ra < 36,420.87) at atmospheric pressure. Vreme et al.[34] studied the gravitational instability triggered by CO_2 dissolution through a water–gas interface with a Hele-Shaw experiment. Lu et al.[35] invented a Hele-Shaw cell that can perform under a high gas pressure of 10 MPa, and experimental results only in the atmosphere pressure were exhibited. Tani[36] established the classical solvability of the one-phase Hele-Shaw problem and justified the vanishing coefficient of the time derivative in the parabolic equation based on Hele-Shaw cell experiments at low pressure. Thomas et al.[37] conducted CO_2 convective dissolution in a Hele-Shaw cell and found that the increase in the salt concentration hindered the development of the instability, increased the wavelength of the convective pattern, and decreased the growth rate and velocity of fingers. Mahmoodpour et al.[38] designed a novel Hele-Shaw cell (2919 < Ra < 4841) and presented the first experiments of dissolution-driven convection of CO_2 in a confined brine-saturated porous medium at pressures up to 3.69 MPa (535.3 psi).

One key issue for the convection experiment with Hele-Shaw cell is the way to detect the variations of CO_2 concentration for visualization purposes. The traditional acid–base indicators cannot capture the full extent of the convection.[39] The research on color indicator demonstrated that the observed patterns and the instabilities may not depend on the presence of a color indicator.[40,41] However, most of the studies visualizing convective patterns with color indicators ignore the concentration.[39]

Micro-schlieren technique is sensitive to the CO_2 concentration based on the deflection of light by a refractive index gradient.[42] Through comparison between the reference and shadowgraph, the noise has been reduced, and the contrast has been improved. The shadow pattern is a light-intensity representation of the low-density regions and high-density regions, which characterizes the well-defined convective flow.[43]

The schlieren images can reflect the changes in the refractive index (n) that is directly related to the density gradient. The relation between density (ρ) and refractive index is described by using the Gladstone–Dale relation[44]

DOI: 10.1021/acsomega.9b00627
ACS Omega 2019, 4, 11082–11092

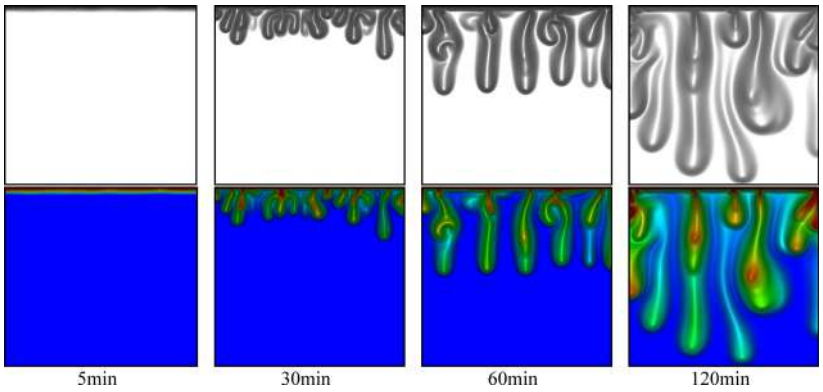

Figure 2. Schlieren images and color schlieren density images of gravitational convection in the Hele-Shaw cell after 5, 30, 60 and 120 min. The view fields of all figures are 1 cm × 1 cm. Blue indicates fresh brine, and the color turns from blue to red with the increase in CO_2 concentrations.

$$n = K_P\rho + 1 \tag{7}$$

where n is the refractive index, ρ is the density, K_P and K_C are the Gladstone–Dale constants, K_P reflects the physical refractive energy, and K_C reflects the chemical refractive energy of fluid. The Gladstone–Dale compatibility, $1 - (K_P/K_C)$, is 0.037 for the ideal formula.

$$K_C = C_i k_i \tag{8}$$

where C_i is the weight percentage of each constituent, and k_i are the specific constants of the chemical data.

PVT Testing. There are a few experimental studies about the convective diffusion in the pressure–volume–temperature (PVT) cell at reservoir conditions.[3] Yang and Gu[45] calculated the CO_2 mass transfer rate in resident brine with a visual high-pressure PVT cell and the pressure decay method. Mojtaba et al.[32] performed quantitative experiments with the PVT cell at elevated pressure and provided an estimation of the convective dissolution of CO_2 in brine. Khosrokhavar[3] studied the CO_2 transfer rate for both fresh brine and brine in pressure constant experiments. The results revealed that the mass transfer rate was much faster than the prediction by Fick's law in the absence of natural convection.

Based on the conservation laws, the total amount of dissolved CO_2 can be calculated as follows

$$n_t = \frac{PV_0}{ZRT} - \frac{PV_t c_t}{ZRT} - \frac{PV_s}{RT}\sum_{t'=0}^{t}\frac{c_{t'}}{Z} \tag{9}$$

where P is the pressure of supercritical fluid in the PVT cell; V_0 and V_t are volumes of supercritical fluid or gas at time 0 and t, respectively; V_s is the sampling volume; c_0 and c_t are concentrations of CO_2 in supercritical fluid or gas at time 0 and t, respectively; Z is the compressibility factor of supercritical fluid or gas; R is the universal gas constant (8.3145 J/(mol·K)); T is the temperature; and t is the diffusion time.

For the pure Fickian diffusion, many researchers[18,46,47] derived separately a same relationship between the mole number of dissolved CO_2 and diffusion coefficient

$$n_t = 2C_s A\sqrt{Dt/\pi} \tag{10}$$

where n_t is the mole number of dissolved CO_2 at time t; A is the area of gas–liquid interface; C_s is the molar concentration or molarity of saturated CO_2 dissolved in liquid. The concentration C_s of saturated CO_2 can be obtained by the following relation

$$C_s = \frac{c_t n_s}{V_s} = \frac{c_t P_0 V_{s0}}{RT_0 V_s} \tag{11}$$

where n_s is the mole number of gas released from the sample at atmospheric pressure, P_0 is the atmospheric pressure, V_{s0} is the volume of the released gas, and T_0 is the temperature of water bath.

According to eq 10, the time-dependent diffusion coefficient was calculated as

$$D = \frac{\pi}{4t}\left(\frac{n_t}{C_s A}\right)^2 \tag{12}$$

Chemical Potential and Reaction Equilibrium. The chemical potential of gaseous or supercritical CO_2 ($scCO_2$) is[48]

$$\mu(g) = \mu^\theta(g) + ZRT\ln(P/P^\theta) + \int_{P^\theta}^{P}(V - ZRT)dP \tag{13}$$

where $\mu(g)$ is the chemical potential of supercritical CO_2, and $\mu^\theta(g)$ is the standard chemical potential, and P^θ is the standard pressure.

The chemical potential of CO_2 in aqueous solution is

$$\mu(aq) = \mu^\theta(aq) + RT\ln(c/c^\theta) \tag{14}$$

Gibbs free energy of solution is[48]

$$G = c_{CO2}G_{CO2} + c_{H2O}G_{H2O} + \Delta H_{mix} - T\Delta S_{mix} \tag{15}$$

where G is the Gibbs free energy, ΔH_{mix} is the enthalpy change, and ΔS_{mix} is the entropy change. The traditional thermodynamic formula is

$$\Delta S_{mix} = -R(c_{CO2}\ln c_{CO2} + c_{H2O}\ln c_{H2O}) \tag{16}$$

CO_2 has much weaker hydrogen bonding than H_2CO_3 to H_2O.[49] When CO_2 dissolves in water, CO_2 undergoes a slight hydration (~0.26%) to H_2CO_3 ($O{=}C(OH)_2$), results in acidic H_2CO_3 ionization, and produces a number of carbonate ions with the following chemical equilibria[2]

$$CO_2(g) + H_2O \leftrightarrow CO_2(aq) + H_2O(1)(slow),$$

$$K = \frac{pCO_2(g)}{[CO_2(aq)]} = 29$$

DOI: 10.1021/acsomega.9b00627
ACS Omega 2019, 4, 11082–11092

$$CO_2(aq) + H_2O(1) \leftrightarrow H_2CO_3(aq)(slow),$$
$$K = \frac{[CO_2(aq)]}{[H_2CO_3]} = 590$$

$$H_2CO_3(aq) + H_2O(l) \leftrightarrow H_3O^+(aq) + HCO_3^-(aq)(fast),$$
$$K = \frac{[H_3O^+][HCO_3^-]}{[H_2CO_3]} = 0.25\ mM$$

$$HCO_3^-(aq) + H_2O(l) \leftrightarrow H_3O^+(aq) + CO_3^{2-}(aq)(fast),$$
$$K = \frac{[H_3O^+][CO_3^{2-}]}{[HCO_3^-]} = 0.047\ nM$$

RESULTS AND DISCUSSION

Visualization Experiments. Figure 2 illustrates the convection processes in the Hele-Shaw experiments. The results were visualized using an optical shadowgraph, which imaged the variation of density via the refraction index.

In the Hele-Shaw experiments, CO_2 started to dissolve as soon as it contacted with the resident brine. The brine with dissolved CO_2 has a higher density than fresh brine.[3] The density of fresh formation water tested with density meters (Anton Paar, DMA HP) is 1.0036 g/mL under reservoir conditions, and the density of CO_2-saturated brine is 1.0275 g/mL. The small increase in brine density is critical to forming convection. It is well known that the Rayleigh−Taylor instability occurs when high-density fluid suspends over lower-density fluid in a gravitational field.[50−52] With the increase in CO_2 concentration, the density increases, which can finally lead to gravitational instabilities in the system.[23]

At the initial stage, the CO_2 dissolution occurred via diffusion on the gas−liquid interface without convection. With the increase in CO_2 concentration in the top fluid, a high-dense planar layer formed and widened rapidly at an almost constant rate. Considering the critical Rayleigh number (Ra_c) as $4\pi^2$, the theoretical critical thickness of the diffusive layer (H_c) is 9.1156 mm, and the corresponding onset time (t_c) is in the range of 2.159−6.238 min. As explained before, convection is impossible when the thickness of the diffusive layer exceeds the critical value.[23] Meanwhile, the gravitational instabilities generated led to tiny disturbances in the diffusive layer sooner.

About half an hour later, the disturbances in the diffusive layer gradually boosted and expanded into distinct plumes under the gravitational instabilities.[53] There was no clear demarcation between the disturbances and plumes. The length of the frontal plumes was measured each time (see Figure 2). The plume length increased with time in nearly linear rather than accelerated transport.

One hour later, the convective plumes were tightly packed with hazy edges when Rayleigh−Taylor convections had developed spontaneously.[18,50] In this step, the plumes carrying CO_2 grew downward and propagated to form many branches and lobes. Meanwhile, most branches died away, and most lobes broke up as CO_2 diffused into the surrounding brine (see Figure 2). With the occurrence of convection, the CO_2 dissolution rate will increase, and the leakage risk will decrease.[10] The width of each plume is varied considerably along the length of the plume, particularly under Rayleigh−Taylor instability. Because Rayleigh−Taylor instability lacks good repetition, we paid more attention to the qualitative law of gravitational convection in the visualization experiments.

Two hours later, the CO_2-dissolved brine vertically streamed down more stably, and the fluid with low CO_2 concentration floated to the top by gravity. The density contrast between CO_2-saturated brine and initial brine is the driving force of plume migration due to the gravitational instabilities.[5] Because the density-driven convection can reduce CO_2 concentration in the gas−liquid interface,[31] the dissolution rate was also enhanced considerably.[33] With the broadening of the convective plumes and the growing amount of CO_2-dissolved brine filling the bottom, the CO_2 concentration at the bottom part of the liquid was noticeably higher than other parts. The boundaries of convective plumes at the bottom blurred gradually to obscurity first. The convective diffusion slowly fell into a decline from bottom to top. Finally, the convective schlieren disappeared as the gravitational convection abated, and the image recovered to the original background.

The visualization experiments illustrated that the gravitational convection creates a more efficient dissolving process by bringing the fresh brine upward to the interface to touch $scCO_2$. The natural convection speeds up the CO_2 dissolution. The gravitational convection plays a significant and positive role in CO_2 geological storage capacity and safety.[27,54]

Influence of Convection on Diffusion Coefficients. Assuming that the diffusive flux is governed by Fick's law with the idealized mass conservation in the PVT system, the saturated solubility of CO_2 in formation water is 5.68×10^{-4} mol/mL under the reservoir conditions (355.65 K, 20.2 MPa). The volume alterations of the supercritical CO_2 with time in the PVT system are shown in Figure 3.

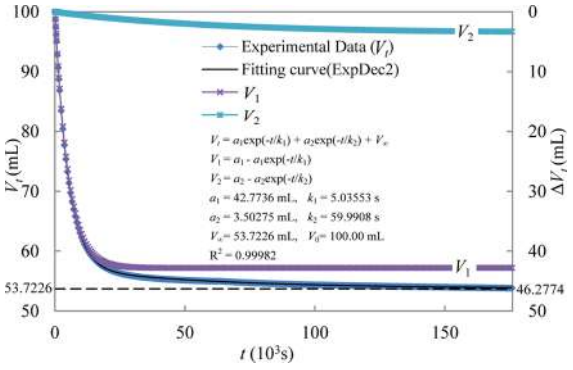

Figure 3. CO_2 volume changed with time during the CO_2 diffusion experiment. The actual value of CO_2 volume in the PVT experiments matches well with the ExpDec2 model,[55] where V_t is the CO_2 volume at time t, t is the diffusive time, a_1 and a_2 are the volume coefficients of the fitting formula, and k_1 and k_2 are the time coefficients of the fitting formula.

In the Fickian diffusion process, CO_2 diffuses into brine and forms a diffusive boundary layer[11] that grows in proportion to the square root of time ($\sqrt{t}$), where perturbations to the stable layer are damped.[5] The relationship curve between the mole number of CO_2 dissolved in resident brines (n_t) and the root of time ($\sqrt{t}$) is drawn in Figure 4.

The curves in Figure 4 are flatter at the initial stage, which indicated that the diffusion was mainly the Fickian diffusion. A study[45] reported that the appearance is caused by gas compression. But the compression has seldom affected our experiments because CO_2 had been pressurized under

DOI: 10.1021/acsomega.9b00627
ACS Omega 2019, 4, 11082−11092

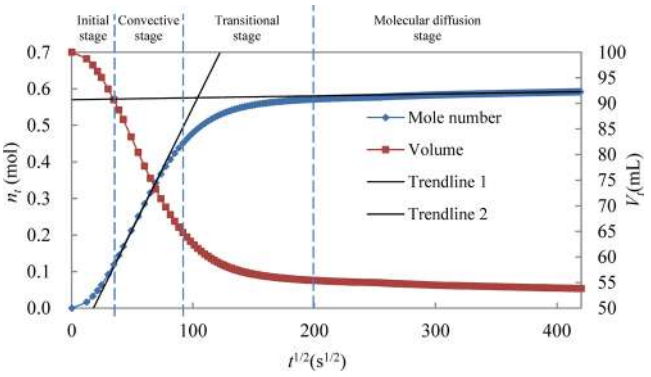

Figure 4. Mole number of CO_2 dissolved in 1 L of brine against the root of time.

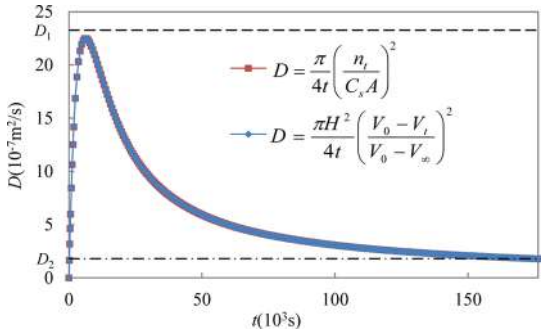

Figure 5. Time-dependent diffusion coefficient curves.

experimental conditions before injecting. The CO_2 diffusion flux (J_t) was dramatically enhanced at the early stage. The diffusion of CO_2 was a faster process at this stage. The CO_2 diffusion coefficient decreased from a maximum of 2.3095 × 10^{-6} m^2/s. The spontaneous convection was considered as the main cause of the acceleration in the CO_2 diffusion rate at the beginning.[18] The dissolution rate slowed down gradually at the transitional stage. The average CO_2 diffusion coefficient is 1.803 × 10^{-7} m^2/s.

The ExpDec2 model can be applied to analyze the data from constant-pressure experiments also. We calculate the diffusion coefficient by fitting pressure-decay data in Figure 3 with this model[55,56]

$$D = 4H^2/k\pi^2 \tag{17}$$

where k are the coefficients of Zhao's fitting formula[56] obtained by fitting pressure-decay data.

We divide the changes of volume into two parts (Figure 3): V_1 reflects the convective diffusion more, and V_2 is prone to reflect the molecular diffusion. V_1 changed rapidly, and its contribution to diffusion reached 92.4287%. However, variation of V_1 had moderated abruptly after a dozen of hours. V_2 changed placidly and sustainably. Based on eq 17, the diffusion coefficient (D_2) calculated by using k_2 is 1.803 × 10^{-7} m^2/s, which is similar to the average CO_2 diffusion coefficient. The diffusion coefficient (D_1) calculated by using k_1 is 2.328 × 10^{-6} m^2/s.

The time-dependent diffusion coefficient was calculated by the formula

$$D = \frac{\pi H^2}{4t}\left(\frac{V_0 - V_t}{V_0 - V_\infty}\right)^2 \tag{18}$$

According to eqs 12 and 18, the diffusion coefficients were calculated.[18,46] The time-dependent diffusion coefficient curves were drawn in Figure 5.

The CO_2 diffusion coefficient reached a peak of 2.282 × 10^{-6} m^2/s rapidly in the initial period and then dropped below the average diffusion coefficient of 1.803 × 10^{-7} m^2/s (Figure 5). The peak diffusion coefficient is more than D_1 and less than the sum of D_1 and D_2. This means that natural convection decreases with time, similar to the density gradient.

Compared with the molecular diffusion coefficient, the average diffusion of CO_2 in brine has improved. Apart from the Fickian diffusion, the average diffusion coefficient of CO_2 is also controlled by chemical reactions and dispersion.[57] Table 1 lists the diffusion coefficients of different ions calculated on the basis of the data reported by Ellis et al.[58]

Effect of Pressure on Gravitational Convection. Table 2 presents the CO_2 saturated solubility (C_s), density (ρ), compressibility factor (Z), volumetric factor (V_f/V_s), average diffusion coefficient (D_a), molecular diffusion coefficient (D_m), normalized Rayleigh number (Ra), and normalized critical time (t_c) in the PVT experiments under pressures in the range of 14−24 MPa.

The saturated solubility of CO_2 in brine increased with pressure. Henry's law indicates that the gaseous CO_2 solubility is linear with respect to pressure. Upon exceeding the critical pressure (7.383 MPa), the solubility of supercritical CO_2 increased sharply with pressure. For the pressure in the range of 14−24 MPa, the elevated pressure enhances CO_2 solubility with lower increment (Table 2). This can be explained by CO_2 chemical potential energy. The chemical potential[48] of CO_2 in the supercritical state μ(sc) increased with pressure greater than that in the melted state μ(aq). The Gibbs energy decreases during elevating pressure ($\Delta G < 0$); more CO_2 molecules can diffuse spontaneously from the supercritical phase into the aqueous phase.

According to molecular dynamics, the molecular diffusion coefficient is proportional to the mean free path of a CO_2 molecule, which decreased with pressure ($D_m \propto P^{-1}$). For self-diffusion at different pressures but the same temperature, the following empirical equation has been suggested[59]

$$\frac{D_m(P_1)}{D_m(P_2)} = \frac{\rho_g(P_2)}{\rho_g(P_1)} = \frac{Z(P_1)/P_1}{Z(P_2)/P_2} \tag{19}$$

where ρ_g is the density of CO_2, and P_1 and P_2 are the corresponding pressures.

The molecular diffusion coefficient (D_m) decreases with pressure. On the contrary, the average diffusion coefficient (D_a) increases with pressure (Table 2).

The density of CO_2-rich brine also increases with pressure. The CO_2 dissolution increasing with pressure is a main reason to increase the density of solution, although the volume also changes.

The pressure affects the density-driven convection.[19] According to eq 1, the Rayleigh number depends on the excess density and diffusion coefficient, both of which are affected by pressure. The pressure has a larger influence on CO_2 solubility and density than diffusion coefficient at the reservoir conditions. Thus, the excess density increases with pressure to enhance the proneness to form gravitational convection.

DOI: 10.1021/acsomega.9b00627
ACS Omega 2019, 4, 11082−11092

Table 1. Molecular Diffusion Coefficients of Different Ions in Brine at 355.65 K

species	D_m ($\times 10^{-9}$ m^2/s)	species	D_m ($\times 10^{-9}$ m^2/s)	species	D_m ($\times 10^{-9}$ m^2/s)
H^+	27.23868	CO_2	5.674726	HCO_3^-	3.627144
OH^-	15.38611	H_2CO_3	4.387674	CO_3^{2-}	2.831513

Table 2. Experimental Parameters with Pressures in the Range of 14−24 MPa (355.65 K)

P (MPa)	C_s (10^4 mol/mL)	ρ (g/L)	Z	V_f/V_s	D_a (10^{-7} m^2/s)	D_m (10^{-9} m^2/s)	Ra	t_c
14.0	5.2940	1.0259	0.5854	1.0053	1.7767	9.0415	0.9449	1.1198
15.0	5.4286	1.0264	0.5639	1.0048	1.7823	8.1306	0.9662	1.0710
16.0	5.5289	1.0268	0.5485	1.0043	1.7875	7.4129	0.9813	1.0382
17.0	5.5951	1.0271	0.5380	1.0039	1.7903	6.8436	0.9914	1.0173
18.0	5.6338	1.0273	0.5318	1.0036	1.7931	6.3890	0.9965	1.0068
19.0	5.6612	1.0274	0.5292	1.0033	1.7977	6.0234	0.9989	1.0020
20.0	5.6795	1.0275	0.5297	1.0031	1.8024	5.7271	0.9997	1.0005
20.2	5.6840	1.0275	0.5308	1.0030	1.8039	5.6747	1.0000	1.0000
21.0	5.6999	1.0276	0.5326	1.0029	1.8060	5.4848	1.0011	0.9977
22.0	5.7159	1.0276	0.5376	1.0027	1.8095	5.2847	1.0023	0.9955
23.0	5.7342	1.0277	0.5443	1.0026	1.8136	5.1179	1.0029	0.9941
24.0	5.7525	1.0278	0.5524	1.0024	1.8183	4.9771	1.0036	0.9927

Table 3. Experimental Parameters with Temperatures in the Range of 293.15−423.15 K (20.2 MPa)

T (K)	C_s (10^4 mol/mL)	ρ (g/L)	Z	V_f/V_s	D_a (10^{-7} m^2/s)	D_m (10^{-9} m^2/s)	Ra	t_c
293	7.2989	1.0354	0.3896	1.0053	1.3353	3.0884	1.8438	0.2941
303	6.8427	1.0330	0.3966	1.0048	1.4042	3.3059	1.6434	0.3702
313	6.4892	1.0314	0.4066	1.0043	1.4741	3.5587	1.4844	0.4538
323	6.2497	1.0303	0.4213	1.0039	1.5454	3.8654	1.3637	0.5376
333	6.0216	1.0292	0.4426	1.0036	1.6172	4.2502	1.2549	0.6349
343	5.8391	1.0283	0.4717	1.0034	1.6915	4.7359	1.1639	0.7381
353	5.7251	1.0277	0.5089	1.0032	1.7653	5.3347	1.0932	0.8365
358	5.6840	1.0275	0.5308	1.00311	1.8037	5.6747	1.0624	0.8859
363	5.6886	1.0274	0.5523	1.00307	1.8413	6.0371	1.0412	0.9223
373	5.6909	1.0273	0.5971	1.00305	1.9172	6.7985	1.0000	1.0000
383	5.7023	1.0272	0.6419	1.00303	1.9957	7.6046	0.9629	1.0783
393	5.7137	1.0271	0.6867	1.00302	2.0744	8.4562	0.9281	1.1610

Effect of Temperature on Gravitational Convection. Table 3 presents the CO_2 saturated solubility, density, compressibility factor, volumetric factor, average diffusion coefficient, molecular diffusion coefficient, normalized Rayleigh number, and normalized critical time with temperature varied in the range of 293.15−423.15 K.

Because of the reservoir pressure above the critical pressure of CO_2 (7.383 MPa), the CO_2 in liquid will be converted into the supercritical state when the temperature is beyond the critical point (304.21 K). For CO_2 in liquid, the saturated solubility in brine decreases with temperature. Because the Gibbs energy (G) increases with temperature (eq 18), dissolution reaches equilibrium earlier under higher temperature. For CO_2 in the supercritical state, the saturated solubility turns from decreasing to increasing with temperature, which is similar to the variation tendency of volumetric factor.

According to molecular dynamics, the molecular diffusion coefficient increases with temperature as $D_m \propto T^{3/2}$. The average diffusion coefficient also increases with temperature (Table 3) because all the diffusion coefficients of different ions increase with temperature.

The Rayleigh number depends on the excess density and diffusion coefficient, which are both affected by temperature. The temperature has a larger influence on diffusion coefficient than the density difference between CO_2 solution and brine at the reservoir conditions. Thus, the diffusion coefficient increases with temperature to enhance the proneness to form gravitational convection.

Further Discussion in Numerical Simulation. This study has been applied to evaluate and predict the productivity of CO_2 flooding and the carbon storage in a Chinese oilfield. After long-term water flooding in this oilfield, the residual oil saturation was 30−35%, the water cut had already reached 98%, and the total recovery percentage had reached 51.52%, which was 99.46% of water flooding recoverable reserves in 2009. The CO_2 flooding has come into the phase of industrialized application since 2010 after its field experiment for 2 years. The CO_2 flooding was mainly conducted by crestal injection.

A precise reservoir geological modeling[60] was set up and applied (see Figure 6a,b). During the reservoir numerical simulation, a convective diffusion model was built based on our result and used to simulate the CO_2 diffusion in brine. The CO_2 diffusion in oil was simulated with a multicomponent diffusion model. Compared with traditional diffusion model, this model can result in dissolved CO_2 that tends to diffuse toward the bottom caused by gravitational convection, which has been proved by CO_2 production data (see Figure 6c,d).

CONCLUSIONS

Visualized experiments with a Hele-Shaw cell were performed to study the gravitational instabilities and their effect on

DOI: 10.1021/acsomega.9b00627
ACS Omega 2019, 4, 11082−11092

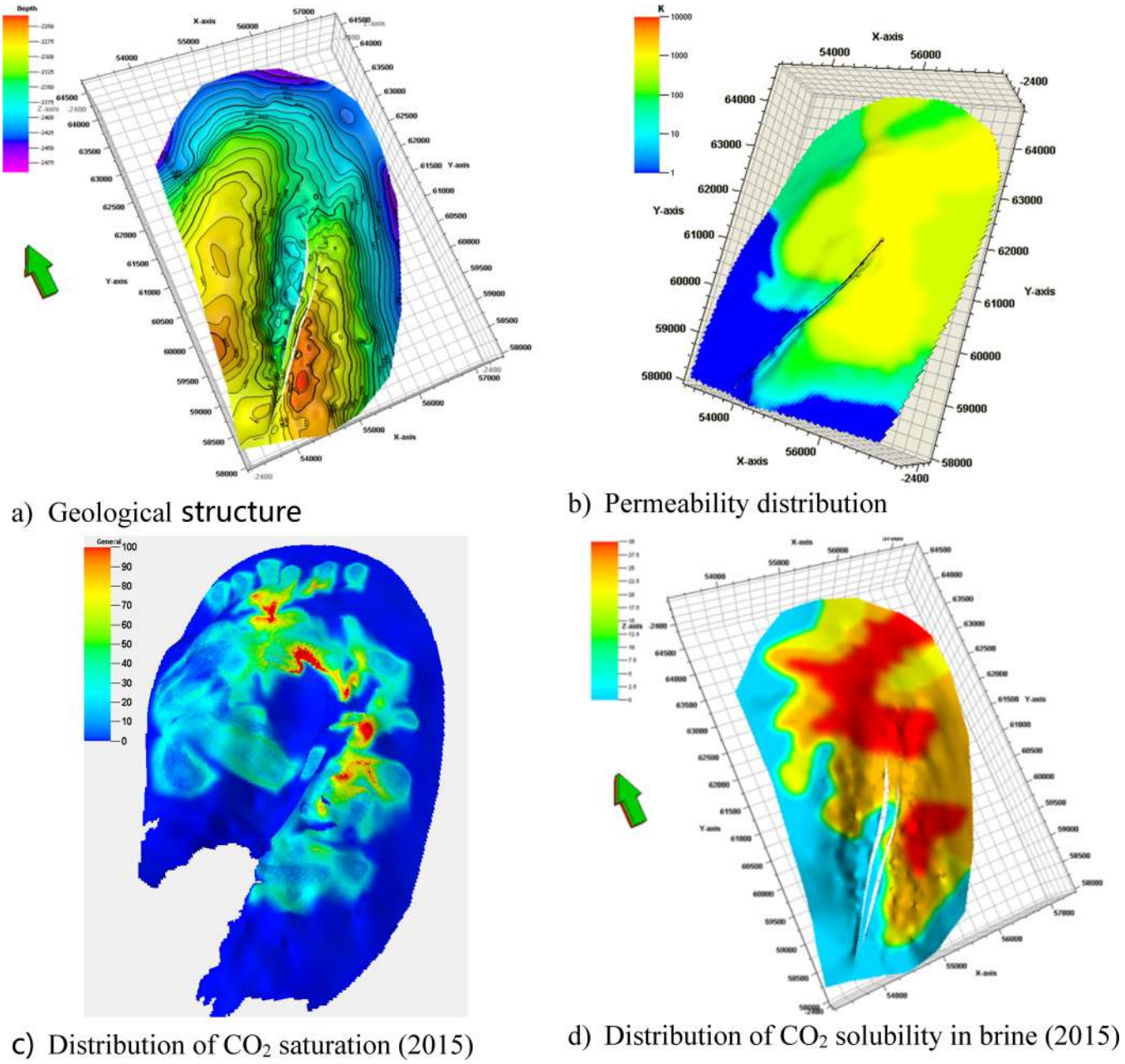

Figure 6. (a–d) Precise 3D reservoir model of Pucheng Oilfield built by Petrel with a grid step size of 50 m.

diffusion rate. The disturbances in the diffusive layer gradually boosted and expanded into convection under the gravitational instabilities. The convective currents triggered by density gradient remarkably enhanced the CO_2 dissolution rate. The density-driven convection further enhances the geological trapping potential. The quantitative experiments in a PVT cell were conducted to investigate the effect of density-driven convection on CO_2 diffusion coefficient by the constant-pressure method. The results demonstrate that the CO_2 diffusion coefficient peaks at early times via the natural convection and higher than the molecular diffusion coefficient. The CO_2 diffusion coefficient was then reduced to approach the average diffusion coefficient with time, which means that the natural convection decreases with time, similar to the density gradient. The PVT experiments were carried out at the temperatures of 293.15−423.15 K and pressures of 14−24 MPa to quantitatively test the influence of temperature or pressure. The results imply that the Rayleigh number increases with pressure and the onset time decreases with pressure. The pressure has a larger influence on CO_2 solubility and density than diffusion coefficient at the reservoir conditions. Thus, the excess density increases with pressure to enhance the proneness to form gravitational convection. The temperature has a larger influence on the diffusion coefficient than the density difference between CO_2 solution and brine at the reservoir conditions. Thus, the diffusion coefficient increases with temperature to enhance the proneness to form gravitational convection. Therefore, the gravitational convection is more likely to occur under greater pressure or higher temperature.

DOI: 10.1021/acsomega.9b00627
ACS Omega 2019, 4, 11082−11092

EXPERIMENTAL SECTION

Materials and Conditions. The PVT testing was carried out under the formation conditions, with an average formation temperature of 355.65 K and formation pressures of 15−24 MPa (average, 20.2 MPa).[2] The $scCO_2$ used in this work is included in Table 4. Resident brine provided by the oilfield has a salinity of above 240 g/L. The ionic composition is listed in Table 5.[2] The viscosity tested with a VISCO 3-1000 LT viscometer (Core Laboratories S.T., USA) is 1.0903 mPa·s at standard conditions (T = 293.15 K, P = 0.1 MPa) and 0.5092 mPa·s at reservoir conditions (355.65 K, 20.2 MPa). The densities tested with density meters (Anton Paar, DMA HP) are 1.1989 g/mL at standard conditions and 1.0036 g/mL at reservoir conditions.

Table 4. CAS Registry Number and Mass Fraction Purity of Gas

component	CAS reg. no.	supplier	mass fraction
CO_2	124-38-9	Beijing Huayuan Gas Chemical Industry Co., Ltd.	>0.990

Visualization Experiments. To better understand the gravitational instabilities and convective instabilities, visualization experiments were conducted in a Hele-Shaw cell at reservoir conditions.[32] The convective behavior in the Hele-Shaw cell is governed by the same law as in porous media.

Experimental Apparatus. A vertically oriented Hele-Shaw cell apparatus, rated to 70 MPa and 473.15 K, was designed independently to study the diffusion and convection characteristics of CO_2 qualitatively (in Figure 7). Similar to the microvisualization experiment apparatus,[61] the Hele-Shaw cell apparatus consists of flat quartz models, a high-pressure holder, flow system, and image acquisition and analysis system. The models with a size of 8 cm × 8 cm × 4 mm have interior rectangular chambers with a size of 4 cm × 4 cm and cell aperture thickness (b) of 0.2 mm. For the Hele-Shaw model with uniform aperture thickness, the Rayleigh number (Ra) is 173.23, and the corresponding permeability (K) is 3333 μm^2 under the reservoir conditions (355.65 K, 20.2 MPa). The model remains vertical in the gravity field and is fitted rigidly in the pressure holder under surrounding pressure created by injecting deionized water. The model has a top outlet and bottom outlet to connect with the pressure holder. The injecting pressure, surrounding pressure, and back pressure were generated and controlled with Quizix pumps within ±0.01 kPa. The temperature of the cell was measured with a calibrated thermocouple and controlled by an electric heating system within ±0.01 K. The pressure holder has sapphire windows for visualization. The images are taken with a transmitted light image acquisition system composed of a Phantom Miro-M320S camera, microscope, LED light tablet, relative analysis software, etc. The image acquisition and analysis system is capable of recording 1320 frames per second (fps) at its resolution of 1920 × 1200 pixels.[61]

Experimental Procedure. After vacuuming the whole system, the pressure holder was filled with deionized water, and the Hele-Shaw cell was filled with formation water from the bottom outlet. Before each measurement, the entire system had been heated to formation temperature (355.65 K). We injected CO_2 into the Hele-Shaw cell from the top outlet to form a CO_2−water interface at the upper of the model and discharged formation water from the bottom outlet back into the brine container. The camera was adjusted to keep the upper boundary of the visual area to coincide with the gas−water interface. The surrounding pressure and model pressure were pressurized to formation pressure (20.2 MPa) and remained constant with the Quizix pumps. Based on the advanced refraction imaging technique,[39] the CO_2 convection images were taken with the transmitted light imaging system. The CO_2 concentration images of high accuracy and resolution were inferred from transmitted light intensity according to the micro-schlieren technique.

Quantitative PVT Experiments. *Experimental Apparatus.* We used a PVT apparatus (Core Laboratories S.T., USA) to study the characteristics of CO_2 dissolution and diffusion in formation water at temperatures of 293.15−423.15 K and pressures of 14−24 MPa. The apparatus is illustrated in Figure 8. The PVT cell has a total sample volume of 240 mL and is rated to 150 MPa and 473.15 K.[62] A visible sapphire window was attached to the front of the cell to obtain full visibility of all the contents, and a magnetic stirrer was equipped on the other side of the cell. The pressure generated with an automatic pump was tested with pressure sensors and controlled with a pressure regulator (CPS) within ±10 kPa. The temperature of the PVT cell was measured by using a calibrated thermocouple and controlled with an electric heating system within ±0.01 K. The volume of the gaseous phase in the PVT cell was measured with a camera-based measurement system (CCD) with the accuracy of 0.0001 mL. We used a GAS 4000 gasometer (Core Laboratories S.T., USA) with 0.001 mL resolution to accurately measure the gas volume at atmospheric pressure.

Experimental Procedure. For quantitative analysis of the CO_2 diffusion, the diffusion of CO_2 in resident brines is tested with the constant-pressure method to provide more accurate (within 0.01%[62]) results by taking into account the liquid phase swelling[4] and unaffected by CO_2 compression.[47] For the constant-pressure method, the diffusion coefficient is calculated by the changes in volume recorded during CO_2 dissolution and diffusion at constant temperature and pressure.[63−66]

Before starting, a leakage test with nitrogen gas was done to ensure that there is no leakage in the system. The formation water and CO_2 were heated to experimental temperature and pressurized to experimental pressure. After vacuuming the system's inner space, a given volume of formation water sample was pressurized into the vertical PVT cell under experimental pressure. Meanwhile, the cell was loaded with the same pumping speed. A sufficient amount of CO_2 was then injected into the PVT cell under experimental conditions. After stopping CO_2 from drawing in, the carried pressure remained constant via the precision pressure regulator. The volume (V) of the cell was measured with CCD system and continuously

Table 5. Ionic Composition of Formation Water (mg/L)

Na^+, K^+	Ca^{2+}	Mg^{2+}	Cl^-	SO_4^{2-}	HCO_3^-	CO_3^{2-}	total
90,452	32,989	4325	92,440	6985	8985	967	243,143

DOI: 10.1021/acsomega.9b00627
ACS Omega 2019, 4, 11082−11092

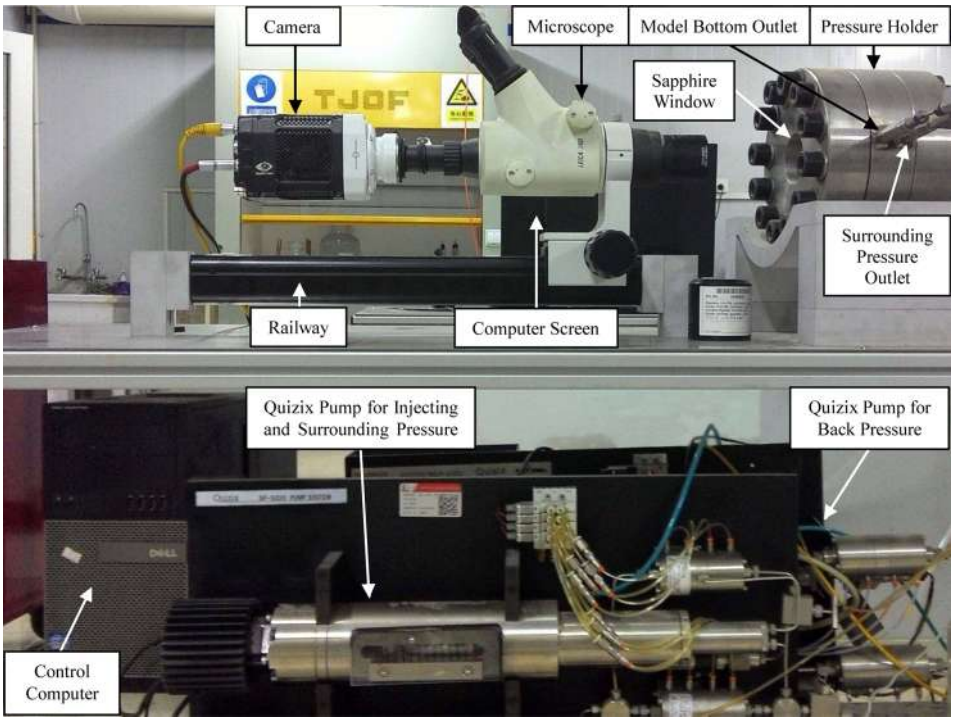

Figure 7. Photograph of the Hele-Shaw cell apparatus.

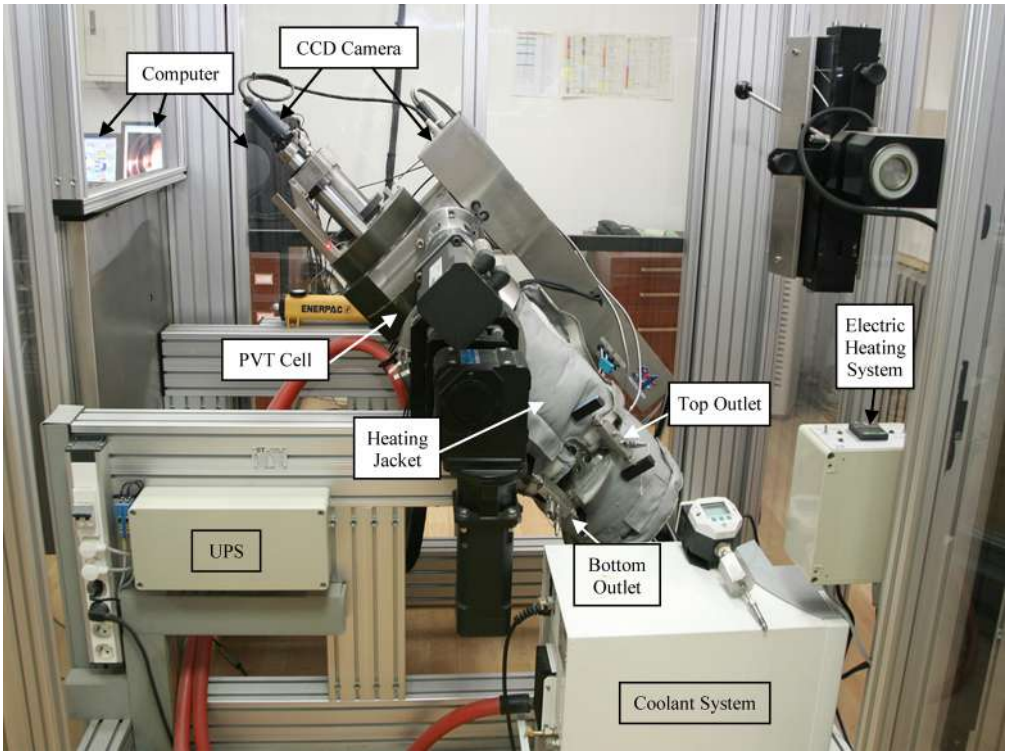

Figure 8. Photograph of the PVT apparatus.

recorded.[62] Some gas phase samples were taken from a top valve with a vacuumed 1 mL flash separator tank (FST). After the tank with the sample was cooled in the water bath, the gas volume at atmospheric pressure was measured with the gasometer for calculating the compressibility factor (Z_t). The gasometer was connected to a gas chromatography spectrometer (Waters, USA) for measuring CO_2 volume concentration in gas (c_t). The diffusion experiment was maintained until the system had reached a thermodynamic equilibrium, as indicated by the volume. Some liquid phase samples were taken from a bottom valve and slowly charged into a vacuumed FST. During the charging process, a needle backpressure valve (with a dead volume of 0.178 mL) was used to avoid pressure decrease. The charged liquid sample (M) was weighted using a precision balance (Mettler Toledo, USA) with an accuracy of 0.001 g for calculating the density (ρ). After cooling in the water bath, the

DOI: 10.1021/acsomega.9b00627
ACS Omega 2019, 4, 11082−11092

gas volume (V_{s0}) was measured with the gasometer at atmospheric pressure. The CO_2 concentration in evolved gases ($c_{t'}$) was measured with the gas chromatography spectrometer (Waters, USA).

AUTHOR INFORMATION

Corresponding Author

*E-mail: luyu@btbu.edu.cn.

ORCID

Yu Lu: 0000-0002-8763-1360

Funding

The authors greatly appreciate the financial support of National Key R&D Program of China (grant no. 2016YFB0600805-1), the National Natural Science Foundation of China (grant no. 51504283), and the Technology Development Department of SINOPEC.

Notes

The authors declare no competing financial interest.

REFERENCES

(1) Brewer, P. G.; Friederich, G.; Peltzer, E. T.; et al. Direct experiments on the ocean disposal of fossil fuel CO_2. *Science* **1999**, *284*, 943−945.

(2) Tang, Y.; Lv, C.; Wang, R.; Cui, M. Mineral dissolution and mobilization during $_{CO\ 2}$ injection into the water-flooded layer of the Pucheng Oilfield, China. *J. Nat. Gas Sci. Eng.* **2016**, *33*, 1364−1373.

(3) Khosrokhavar, R. *Effect of Salinity and Pressure on the Rate of Mass Transfer in Aquifer Storage of Carbon Dioxide*; Springer International Publishing: 2016, *59*, 57−82.

(4) Khosrokhavar, R.; Elsinga, G.; Farajzadeh, R.; Bruining, H. Visualization and Investigation of Natural Convection Flow of CO_2 in Aqueous and Oleic Systems. *J. Pet. Sci. Eng.* **2014**, *122*, 230−239.

(5) Islam, A. W.; Meckel, T. A.; Sun, A. Y.; et al. Numerical experiments of density driven CO_2 saturated brine migration in heterogeneous two-dimensional geologic fabric materials. *Int. Commun. Heat Mass Transfer* **2016**, *71*, 148−156.

(6) Dorao, C. A. Dispersion phenomena in gas liquid systems. *J. Nat. Gas Sci. Eng.* **2012**, *5*, 25−30.

(7) Emami-Meybodi, H. Stability analysis of dissolution-driven convection in porous media. *Phys. Fluids* **2017**, *29*, No. 014102.

(8) Emami-Meybodi, H.; Hassanzadeh, H. Two-phase convective mixing under a buoyant plume of CO_2 in deep saline aquifers. *Adv. Water Resour.* **2015**, *76*, 55−71.

(9) Soltanian, M. R.; Amooie, M. A.; Dai, Z.; et al. Critical Dynamics of Gravito-Convective Mixing in Geological Carbon Sequestration. *Sci. Rep.* **2016**, *6*, 35921.

(10) Kong, X.-Z.; Saar, M. O. Numerical study of the effects of permeability heterogeneity on density-driven convective mixing during CO_2 dissolution storage. *Int. J. Greenhouse Gas Control* **2013**, *19*, 160−173.

(11) Martinez, M. J.; Hesse, M. A. Two-phase convective CO2dissolution in saline aquifers. *Water Resour. Res.* **2016**, *52*, 585−599.

(12) Islam, A.; Sun, A. Y.; Yang, C. Reactive Transport Modeling of the Enhancement of Density-Driven CO_2 Convective Mixing in Carbonate Aquifers and its Potential Implication on Geological Carbon Sequestration. *Sci. Rep.* **2016**, *6*, 24768.

(13) Chao, Y.; Mak, S. Y.; Ma, Q.; et al. Emergence of Droplets at the Nonequilibrium All-Aqueous Interface in a Vertical Hele-Shaw Cell. *Langmuir* **2018**, *34*, 3030−3036.

(14) Liyanage, R.; Crawshaw, J.; Krevor, S.; et al. Multidimensional Imaging of Density Driven Convection in a Porous Medium. *Energy Procedia* **2017**, *114*, 4981−4985.

(15) Teng, Y.; Lu, G.; Fan, Y.; et al. Experimental Study of Density-driven Convection in Porous Media by Using MRI. *Energy Procedia* **2017**, *105*, 4210−4215.

(16) Nield, D. A.; Bejan, A. *Convection in Porous Media*. Springer: Berlin, 2013, *108*(2), 284−290.

(17) Gubbins, D. The Rayleigh number for convection in the Earth's core. *Phys. Earth Planet. Inter.* **2001**, *128*, 3−12.

(18) Slim, C. A.; Bandi, M. M.; Miller, C. J.; et al. Dissolution-driven convection in a Hele-Shaw cell. *Phys. Fluids* **2013**, *25*, 024101.

(19) Faisal, T. F.; Chevalier, S.; Bernabe, Y.; et al. Quantitative and qualitative study of density driven CO_2 mass transfer in a vertical Hele-Shaw cell. *Int. J. Heat Mass Transfer* **2015**, *81*, 901−914.

(20) Ennis-King, J. P.; Paterson, L. Role of Convective Mixing in the Long-Term Storage of Carbon Dioxide in Deep Saline Formations. *SPE Journal* **2013**, *10*, 349−356.

(21) Nield, D. A. Onset of Thermohaline Convection in a Porous Medium. *Water Resour. Res.* **1968**, *4*, 553−560.

(22) Slim, A. C.; Ramakrishnan, T. S. Onset and cessation of time-dependent, dissolution-driven convection in porous media. *Phys. Fluids* **2010**, *22*, 124103.

(23) Szulczewski, M. L.; Hesse, M. A.; Juanes, R. Carbon dioxide dissolution in structural and stratigraphic traps. *J. Fluid Mech.* **2013**, *736*, 287−315.

(24) Slim, A. C. Solutal-convection regimes in a two-dimensional porous medium. *J. Fluid Mech.* **2014**, *741*, 461−491.

(25) Kneafsey, T. J.; Pruess, K. Laboratory flow experiments for visualizing carbon dioxide-induced, density-driven brine convection. *Transp. Porous Media* **2010**, *82*, 123−139.

(26) Hassanzadeh, H.; Pooladi-Darvish, M.; Keith, D. W. Scaling behavior of convective mixing, with application to geological storage of CO_2. *AIChE J.* **2007**, *53*, 1121−1131.

(27) Teng, Y.; Jiang, L.; Fan, Y.; et al. Quantifying the dynamic density driven convection in high permeability packed beds. *Magn. Reson. Imaging* **2017**, *39*, 168−174.

(28) Lindeberg, E.; Wessel-Berg, D. Upscaling studies of diffusion induced convection in homogeneous and heterogeneous aquifers. *Energy Procedia* **2011**, *4*, 3927−3934.

(29) Farajzadeh, R.; Salimi, H.; Zitha, P. L. J.; et al. Numerical Simulation of Density-Driven Natural Convection in Porous Media with Application for CO_2 Injection Projects. *Int. J. Heat Mass Transfer* **2007**, *50*, 5054−5064.

(30) Hele-Shaw, H. S. The Motion of a Perfect Liquid. *Nature* **1899**, *1558*, 446−451.

(31) Backhaus, S.; Turitsyn, K.; Ecke, R. E. Convective Instability and Mass Transport of Diffusion Layers in a Hele-Shaw Geometry. *Phys. Rev. Lett.* **2011**, *106*, 104501.

(32) Mojtaba, S.; Behzad, R.; Rasoul, N. M.; et al. Experimental study of density-driven convection effects on CO_2 dissolution rate in formation water for geological storage. *J. Nat. Gas Sci. Eng.* **2014**, *21*, 600−607.

(33) Vosper, H.; Kirk, K.; Rochelle, C.; et al. Does numerical modelling of the onset of dissolution- convection reliably reproduce this key stabilization process in CO_2 Storage? *Energy Procedia* **2014**, *63*, 5341−5348.

(34) Vreme, A.; Nadal, F.; Pouligny, B.; et al. Gravitational instability due to the dissolution of carbon dioxide in a Hele-Shaw cell. *Phys. Rev. Fluids* **2016**, *1*, No. 064301.

(35) Lu, G.; Liu, Y.; Jiang, L.; et al. Study of Density Driven Convection in a Hele-Shaw Cell with Application to the Carbon Sequestration in Aquifers. *Energy Procedia* **2017**, *114*, 4303−4312.

(36) Tani, H. Classical Solvability of the Radial Viscous Fingering Problem in a Hele-Shaw Cell with Surface Tension. *J. Math. Sci.* **2018**, *228*, 449−462.

(37) Thomas, C.; Dehaeck, S.; de Wit, A. Convective dissolution of CO_2 in water and salt solutions. *Int. J. Greenhouse Gas Control* **2018**, *72*, 105−116.

(38) Mahmoodpour, S.; Rostami, B.; Soltanian, M. R.; et al. *Convective dissolution of carbon dioxide in deep saline aquifers: Insights from engineering a high-pressure porous Hele-Shaw cell*. Cornell University working paper, 2018, https://arxiv.org/abs/1812.08366.

DOI: 10.1021/acsomega.9b00627
ACS Omega 2019, 4, 11082−11092

(39) Thomas, C.; Lemaigre, L.; Zalts, A.; et al. Experimental study of CO_2 convective dissolution: The effect of color indicators. *Int. J. Greenhouse Gas Control* **2015**, *42*, 525−533.
(40) Almarcha, C.; Trevelyan, P. M. J.; Riolfo, L. A.; et al. Active Role of a Color Indicator in Buoyancy-Driven Instabilities of Chemical Fronts. *J. Phys. Chem. Lett.* **2010**, *1*, 752−757.
(41) Kuster, S.; Riolfo, L. A.; Zalts, A.; et al. Differential diffusion effects on buoyancy-driven instabilities of acid-base fronts: the case of a color indicator. *Phys. Chem. Chem. Phys.* **2011**, *13*, 17295−17303.
(42) Settles, G. S.; Covert, E. E. Schlieren and shadowgraph techniques: Visualizing phenomena in Transport media. *Appl. Mech. Rev.* **2002**, *55*, B76−B77.
(43) Zarabadi, A. S.; Pawliszyn, J.; Hajialamdari, M. Development of a multichannel microfluidic system with Schlieren imaging microscopy for online chip-based moving boundary electrophoresis. *J. Chromatogr. A* **2017**, *1484*, 93−97.
(44) Rantzsch, U.; Kloess, G.; Lange, J. M.; et al. Gladstone-Dale relationship-Application for tektites. *Chem. Erde* **2011**, *71*, 197.
(45) Yang, C.; Gu, Y. Accelerated mass transfer of CO_2 in reservoir brine due to density-driven natural convection at high pressures and elevated temperatures. *Ind. Eng. Chem. Res.* **2005**, *45*, 2430−2436.
(46) Wang, S.; Hou, J.; Liu, B.; et al. The Pressure-decay Method for Nature Convection Accelerated Diffusion of CO2 in Oil and Water under Elevated Pressures. *Energy Sources, Part A* **2013**, *35*, 538−545.
(47) Etminan, S. R.; Maini, B. B.; Chen, Z.; et al. Constant-pressure technique for gas diffusivity and solubility measurements in heavy oil and bitumen. *Energy Fuels* **2010**, *24*, 533−549.
(48) David, C. W. Fugacity Examples 2: The fugacity of a ″hard-sphere″ semi-ideal gas and the van der Waals gas. *Chem. Ed. Mater.* **2015**.
(49) Lam, R. K.; England, A. H.; Smith, J. W.; et al. The hydration structure of dissolved carbon dioxide from X-ray absorption spectroscopy. *Chem. Phys. Lett.* **2015**, *633*, 214−217.
(50) De Paoli, M.; Zonta, F.; Soldati, A. Rayleigh-Taylor convective dissolution in confined porous media. *Phys. Rev. Fluids* 2019, Accepted.
(51) Plesset, M. S.; Winet, H. Bioconvection patterns in swimming microorganism cultures as an example of Rayleigh-Taylor instability. *Nature* **1974**, *248*, 441−443.
(52) Cabot, W. H.; Cook, A. W. Reynolds number effects on Rayleigh-Taylor instability with possible implications for type Ia supernovae. *Nat. Phys.* **2006**, *2*, 562−568.
(53) Tilton, N.; Daniel, D.; Riaz, A. The initial transient period of gravitationally unstable diffusive boundary layers developing in porous media. *Phys. Fluids* **2013**, *25*, 092107.
(54) Teng, Y.; Wang, P.; Liu, Y.; et al. A spectrophotometric method for measuring dissolved CO_2 in saline water. *Exp. Fluids* **2018**, *59*, 138.
(55) Zhao, R.; Ao, W.; Xiao, A.; et al. Diffusion law and measurement of variable diffusion coefficient of CO_2 in oil. *J. China Univ. Pet.* **2016**, *40*, 136−142.
(56) Zhao, R.; Xu, M.; Yang, J.; et al. Non-constant Diffusion Behavior for CO_2 Diffusion into Brine: Influence of Density-Driven Convection. *J. Solution Chem.* **2018**, *47*, 1926−1941.
(57) Ovaysi, S.; Piri, M. Pore-scale dissolution of CO_2+SO_2, in deep saline aquifers. *Int. J. Greenhouse Gas Control* **2013**, *15*, 119−133.
(58) Ellis, B. R.; Crandell, L. E.; Peters, C. A. Limitations for brine acidification due to SO2 co-injection in geologic carbon sequestration. *Int. J. Greenhouse Gas Control* **2010**, *4*, 575−582.
(59) Cussler, E. L. *Diffusion: Mass Transfer in Fluid Systems*, 3rd Edition; Cambridge University Press: New York, NY, USA, 2009, 237−273.
(60) Ren, M. *Research and appliance of horizontal wells drilled high water cut stage of development for remaining oil development in Pucheng Oilfield*. Ph.D thesis of China University of Geosciences, Beijing, 2012.
(61) Cui, M.; Wang, R.; Lv, C.; et al. Research on Microscopic Oil Displacement Mechanism of CO_2, EOR in Extra-high Water Cut Reservoirs. *J. Pet. Sci. Eng.* **2017**, *154*, 315−321.
(62) Yang, Z.; Li, M.; Peng, B.; Lin, M.; Dong, Z. Dispersion property of CO2in oil. 1. volume expansion of CO2+ Alkane at near critical and supercritical condition of CO_2. *J. Chem. Eng. Data* **2012**, *57*, 882−889.
(63) Sun, Q.; Tian, H.; Li, Z.; et al. Solubility of CO_2 in water and NaCl solution in equilibrium with hydrate. Part I: Experimental measurement. *Fluid Phase Equilib.* **2016**, *409*, 131−135.
(64) Crank, J. *The Mathematics of Diffusion*, 2nd edition; Calrendon Press: Oxford, U. K., *47*, 1975.
(65) Bahar, M. M.; Liu, K. Measurement Of The Diffusion Coefficient Of CO_2 In Formation Water Under Reservoir Conditions: Implications For CO_2 Storage. *SPE Asia Pacific Oil and Gas Conference and Exhibition*; Society of Petroleum Engineers: 2008, *390*(1), 91−94.
(66) Gholami, Y.; Azin, R.; Fatehi, R.; et al. Suggesting a numerical pressure-decay method for determining CO_2 diffusion coefficient in water. *J. Mol. Liq.* **2015**, *211*, 31−39.

DOI: 10.1021/acsomega.9b00627
ACS Omega 2019, 4, 11082−11092